Check for updates

Two-Compartment Perfusion MR IVIM Model to Investigate Normal and Pathological Placental Tissue

Alessandra Maiuro, MS,[1,2] Giada Ercolani, MD,[3] Francesca Di Stadio, MS,[1] Amanda Antonelli, MD,[3] Carlo Catalano, MD,[3] Lucia Manganaro, MD,[3] and Silvia Capuani, PhD[2*]

Background: Perfusion and diffusion coexist in the placenta and can be altered by pathologies. The two-perfusion model, where f_1 and, f_2 are the perfusion-fraction of the fastest and slowest perfusion compartment, respectively, and D is the diffusion coefficient, may help differentiate between normal and impaired placentas.
Purpose: Investigate the potential of the two-perfusion IVIM model in differentiating between normal and abnormal placentas.
Study-Type: Retrospective, case–control.
Population: 43 normal pregnancy, 9 fetal-growth-restriction (FGR), 6 small-for-gestational-age (SGA), 4 accreta, 1 increta and 2 percreta placentas.
Field Strength/Sequence: Diffusion-weighted-echo planar imaging sequence at 1.5 T.
Assessment: Voxel-wise signal-correction and fitting-controls were used to avoid overfitting obtaining that two-perfusion model fitted the observed data better than the IVIM model (Akaike weight: 0.94). The two-perfusion parametric-maps were quantified from ROIs in the fetal and maternal placenta and in the accretion zone of accreta placentas. The diffusion coefficient D was evaluated using a $b \geq 200$ sec/mm^2-mono-exponential decay fit. IVIM metrics were quantified to fix $f_1 + f_2 = f_{IVIM}$.
Statistical-Tests: ANOVA with Dunn-Sidák's post-hoc correction and Cohen's d test were used to compare parameters between groups. Spearman's coefficient was evaluated to study the correlation between variables. A P-value<0.05 indicated a statistically significant difference.
Results: There was a significant difference in f_1 between FGR and SGA, and significant differences in f_2 and f_{IVIM} between normal and FGR. The percreta + increta group showed the highest f_1 values (Cohen's $d = -2.66$). The f_2 between normal and percreta + increta groups showed Cohen's $d = 1.12$. Conversely, f_{IVIM} had a small effective size (Cohen's $d = 0.32$). In the accretion zone, a significant correlation was found between f_2 and GA ($\rho = 0.90$) whereas a significant negative correlation was found between f_{IVIM} and D ($\rho = -0.37$ in fetal and $\rho = -0.56$ in maternal side) and f_2 and D ($\rho = -0.38$ in fetal and $\rho = -0.51$ in maternal side) in normal placentas.
Conclusion: The two-perfusion model provides complementary information to IVIM parameters that may be useful in identifying placenta impairment.
Level of Evidence: 2
Technical Efficacy Stage: 1

J. MAGN. RESON. IMAGING 2024;59:879–891.

The placenta is involved in the transfer of oxygen and the exchange of nutrients between the mother and the fetus during pregnancy.[1] The human placenta is hemochorial, meaning that fetal and maternal blood cannot mix.[1] Thus, it is characterized by two separate structures: the chorionic plate, which is the fetal placenta side, and the basal plate

View this article online at wileyonlinelibrary.com. DOI: 10.1002/jmri.28858

Received Mar 15, 2023, Accepted for publication May 30, 2023.

*Address reprint requests: S.C., CNR-ISC, Piazzale Aldo Moro 5, 00185, Rome, Italy. E-mail: silvia.capuani@roma1.infn.it

From the [1]Department of Physics, Sapienza University of Rome, Rome, Italy; [2]Physics Department Rome, CNR ISC Roma Sapienza, Rome, Italy; and [3]Department of Radiological, Oncological and Pathological Sciences, Umberto I Hospital, Sapienza University of Rome, Rome, Italy

Additional supporting information may be found in the online version of this article

This is an open access article under the terms of the Creative Commons Attribution License, which permits use, distribution and reproduction in any medium, provided the original work is properly cited.

© 2023 The Authors. *Journal of Magnetic Resonance Imaging* published by Wiley Periodicals LLC on behalf of International Society for Magnetic Resonance in Medicine.

surrounding the intervillous space, which constitutes the maternal side. The chorionic plate is characterized by the villous trees that are vascularized with fetal blood and exchange nutrients and substances with the surrounding maternal free blood that flows through the intervillous space.[1] The placenta may incur structural and physiological abnormalities such as intrauterine growth restriction (IUGR) and placental accretism.[1]

The placenta accreta is characterized by the absence of the maternal decidua, so the villous trees can proliferate and anchor directly on the myometrium.[1] There are three degrees of abnormal placental infiltration: the placenta accreta where villi do not invade muscles, the increta where villi invade the myometrium and the percreta where villi cross the serous membrane and can infiltrate the bladder or the rectus depending on the position of the accretion zone.[1] The accretion zone is highly perfused, so this pathology could cause hemorrhages during the delivery and could also lead to a hysterectomy.[2]

As placental function is related to the health of the newborn and the future adult,[3,4] the development of noninvasive diagnostic techniques to assess and monitor it is desirable.

IUGR is due to the anomalous trophoblastic invasion of the spiral arteries[1]: the arteries are narrower than in normal subjects, and this causes the maternal placenta's incoming blood to have higher pressure and velocity.[1] Because the fetal-maternal blood exchange occurs at the interphase between the intravillous maternal placenta and the villous membrane (the trophoblast), the oxygenated blood could be more drained than in healthy placentas causing a decrease of the trophoblastic functionality.[1] IUGR fetuses are characterized by an estimated fetal weight (EFW) below the 10th percentile, so they are smaller than healthy normal fetuses and they could develop heart and neurological disease after birth.[5,6] IUGR fetuses may be differentiated into fetal growth restriction (FGR) and small for gestational age (SGA) groups, according to the presence or absence of fetoplacental Doppler abnormalities detected in utero. However, while ultrasound is currently considered the primary diagnostic tool to predict perinatal outcome,[6–8] its imaging and flowmetry cannot assess the micro-perfusive and microstructural placental qualities. MRI may be employed as an alternate method to investigate the placental tissues.[9] In particular, diffusion weighted imaging (DWI) is a powerful technique that provides microstructural information without requiring contrast agents that could result in adverse effects on fetal development.[10]

Given the complexity of biological tissues in which perfusion and diffusion compartments coexist, different models have been developed to approximate the DWI signal.[11] The most widely known and used is the intravoxel incoherent motion (IVIM) model, a bi-exponential model that considers two separate compartments: that of perfusion quantified by the perfusion fraction f_{IVIM} of perfusing molecules at a rate given by the pseudo-diffusion coefficient D^*, and the diffusion compartment quantified by the diffusion coefficient D[12] of $1-f_{\mathrm{IVIM}}$ water molecules. Previous studies have highlighted interesting results of IVIM applied to placenta tissues.[13–16] In the placental tissue, f_{IVIM} quantifies the perfusion fraction of water molecules perfused in microcapillaries with D^* rate, whereas D, which quantifies the hindered diffusion of water molecules in the extracellular space, is related to tissue microstructure. Some authors have identified f_{IVIM} as a biomarker to discriminate between IUGR and normal fetuses[13–15] and to discriminate between normal and accreta placentas.[16] In this study, we hypothesized that, in the placenta, two main perfusion compartments exist in addition to the diffusion compartment, and that the introduction of more parameters describing placental perfusion can provide more information to identify the placenta's physiological and microstructural characteristics and understand the mechanism involved in placental diseases.

Thus, the aim of this study was to investigate the potential of a three compartment (two perfusion and one diffusion) model, based on the two-perfusion model developed by Fournet et al.,[17] to discriminate between normal, SGA, FGR, and accreta placentas.

Materials and Methods

Fig. 1 shows a schematic representation of the pipeline used in this study.

Study Cohort

Following the study's approval by the ethical committee of the Policlinico Umberto I, Sapienza, Rome, Italy, 85 singleton pregnancies with an average gestational age (GA) of 20 ± 2.5 weeks (15–27 weeks) were enrolled from January 2018 to March 2022. All patients completed written consent forms prior to the study. One patient was excluded as it had not a singleton placenta, 19 other patients were excluded because of motion artifacts and signal noise ratio (SNR) lower than 3 a.u. for high b-values. The final study subjects were comprised of 65 patients who were divided into four groups: normal pregnancy (Normal), $n = 43$; FGR, $n = 9$; SGA, $n = 6$, and accreta, $n = 7$. The accreta group consisted of $n = 4$ accreta, $n = 1$ increta, and $n = 2$ percreta (Table 1).

Model

Placenta physiology is characterized by at least two main perfusion compartments: the compartment given by the exchange of substances through the trophoblastic cells between the mother and fetus side and the perfusion compartment related to pumped blood inside the villous trees. It is reasonable to think that the perfusion rate of the two compartments is different by at least one order of magnitude.[18] Moreover, the diffusion compartment in the placenta is mainly due to the blood flowing in the intravillous space.

15222586, 2024, 3, Downloaded from https://onlinelibrary.wiley.com/doi/10.1002/jmri.28858 by Ospedale Santa Lucia, Wiley Online Library on [04/02/2025]. See the Terms and Conditions (https://onlinelibrary.wiley.com/terms-and-conditions) on Wiley Online Library for rules of use; OA articles are governed by the applicable Creative Commons License

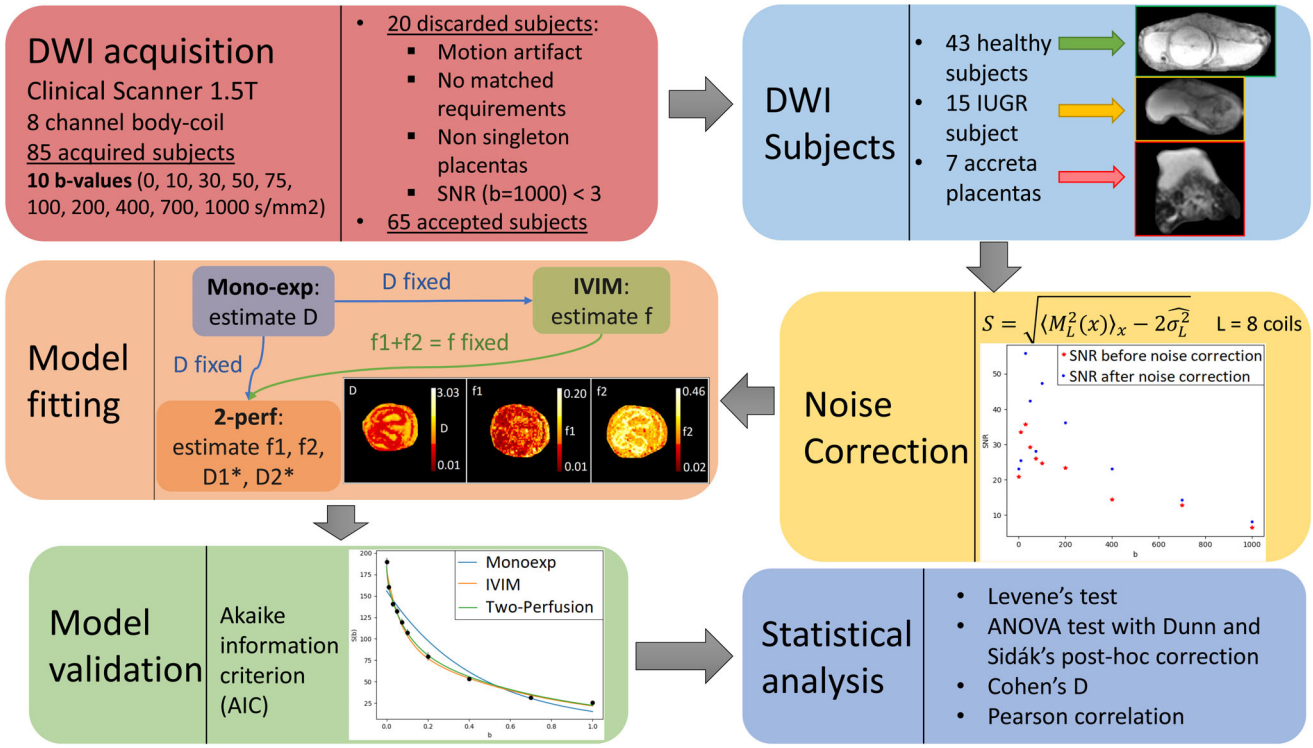

FIGURE 1: Flow-chart of the study.

TABLE 1. Pregnancy Women Cohorts

Patients	Number of subjects	Gestational Age (GA) (weeks)	Upper/Lower limits (weeks)
Normal	43	27.38 ± 0.80	38.00/19.86
FGR	9	27.25 ± 1.86	33.57/19.29
SGA	6	27.00 ± 2.52	35.00/20.00
Accretes (ACC)	7	30.60 ± 2.72	35.57/28.14
Accreta	4	29.71 ± 1.14	30.86/28.57
Increta	1	32.00	–
Percreta	2	31.68 ± 1.93	35.57/28.14

FGR: fetal growth restriction; SGA: small for gestational age.

The model described by Fournet et al.[17] considers the contribution of two vascular pools (capillaries and larger vessels) in rat brains:

$$\frac{S(b)}{S(0)} = f_{\text{fast}} e^{-\left(D^*_{\text{fast}}+D\right)b} + f_{\text{slow}} e^{-\left(D^*_{\text{slow}}+D\right)b} + \left(1 - f_{\text{fast}} - f_{\text{slow}}\right) e^{-Db} \quad (1)$$

The two-perfusion model foresees the presence of diffusion in each compartment and divides perfusion compartments into slow and fast perfusion. We adapted Fournet et al. model[17] to study the placenta tissue adding the slow perfusion contribution to the first fast perfusion compartment:

$$\frac{S(b)}{S(0)} = f_1 e^{-\left(D^*_1+D^*_2+D\right)b} + f_2 e^{-\left(D^*_2+D\right)b} + \left(1 - f_1 - f_2\right) e^{-Db} \quad (2)$$

where D is the pseudo-diffusion coefficient relating to the maternal blood flowing inside the intravillous space, D^*_1 is the fastest pseudo-perfusion coefficient given by the blood

15222586, 2024, 3, Downloaded from https://onlinelibrary.wiley.com/doi/10.1002/jmri.28858 by Ospedale Santa Lucia, Wiley Online Library on [04/02/2025]. See the Terms and Conditions (https://onlinelibrary.wiley.com/terms-and-conditions) on Wiley Online Library for rules of use; OA articles are governed by the applicable Creative Commons License

flowing inside microvessels and villous trees, D_2^* is the slower pseudo-perfusion coefficient given by the exchange of nutrients between the maternal and the fetal compartments, f_1 is the fastest perfusion fraction and f_2 is the slowest perfusion fraction related to the trophoblastic cells. The choice to add D_2^* in the fast perfusion compartment was because it could not be distinguished from the fastest D_1^* relating to the villi's vasculature, thus D_2^* should contribute to the actual fast perfusion compartment.

To reduce the number of free parameters, the diffusion coefficient D was estimated by fitting a mono-exponential model at high b-value $\left(b \geq 200 \frac{s}{mm^2}\right)$ to DWI data. Since the placenta has two well-defined perfusion processes contributing to the global perfusion, the IVIM model was used to obtain the total perfusion fraction $f_{\text{IVIM}} = f_1 + f_2$. Therefore, the resulting model used in this work is:

$$S(b) = S(0)\Big(f_1 e^{-\left(D_1^* + D_2^* + D_{\text{mono}}\right)b} + \left(f_{\text{IVIM}} - f_1\right)e^{-\left(D_2^* + D_{\text{mono}}\right)b} + \left(1 - f_{\text{IVIM}}\right)e^{-D_{\text{mono}}b}\Big) \tag{3}$$

where f_{IVIM} and D_{mono} (the D estimated by a mono-exponential model) are fixed. All the models were fitted to DWI data using a homemade Python script using a nonlinear least-squares algorithm.

Data Acquisition

DWIs were acquired using a 1.5 T Siemens Avanto (Erlangen, Germany) clinical scanner with an eight-channel body coil without any parallel MRI reconstruction techniques. The acquisition protocol consisted of a diffusion weighted echo-planar imaging spin echo sequence with TR/TE = 3900/74.8 msec, bandwidth 1184 Hz/px, matrix size of 192 × 192, FOV = 220 × 220 mm^2, slice thickness of 5 mm, and 18 to 30 slices, depending on the placenta's size. The diffusion encoding gradients were applied along three non-coplanar directions using 10 different b-values (0, 10, 30, 50, 75, 100, 200, 400, 700, and 1000 sec/mm^2), and the signal over the three directions was averaged. The number of averaged signals was NS = 4 for each b-value, thus the total duration of the protocol was ~15 minutes.

Preprocessing

The maternal and fetal sides of placentas were analyzed. Given the complexity of the placental tissue, six regions of interest (ROI) were manually delineated on the fetal and maternal sides by two different radiology specialists both of 5 years of experience (all results relating to these six regions are available in the Supplemental Material). In accreta placentas the ROI was delineated on the accretion zone.

In multiple-coil acquisition, the noise is known to follow a noncentral χ distribution, which collapses in a χ distribution on the background with a number of degrees of freedom relying on the coils' number.[19] The noise was estimated using the following estimator based on local moments[19]:

$$\widehat{\sigma_L^2} = \frac{1}{2}\text{mode}\left\{\left\langle M_L^2(x)\right\rangle_x\right\} \tag{4}$$

where $\left\langle M_L^2(x)\right\rangle_x$ is the local mean of the corrupted squared signal calculated using a local window size 21 × 21, $\widehat{\sigma_L^2}$ is the estimated squared noise of the image, and L is the number of coils. In clinical scanners, row data are already filtered by default with a weak filter, which is of an unknown type because it is protected by manufacturing company licenses. Hence, the exact noise distribution is unknown. In this study, therefore, the "mode" has been approximated as the maximum of the signal intensity histogram, and the resulting corrected signal is given by[19]:

$$S = \sqrt{\left\langle M_L^2(x)\right\rangle_x - 2\widehat{\sigma_L^2}} \tag{5}$$

where the corrupted signal's second order $\left\langle M_L^2(x)\right\rangle_x$ was calculated over every single ROI for the analysis of the tissue. Diffusion and perfusion parametric maps were obtained by first performing a voxel-wise signal correction, where $\left\langle M_L^2(x)\right\rangle_x$ was estimated by implementing a 2 × 2 filter on each voxel (example shown in Fig. 2). Then, the two-perfusion IVIM model was fitted using a bugged trees algorithm provided by MATLAB's machine learning official toolbox (MATLAB R2021a). In particular, the bugged trees are built by the function *TreeBagger()*, then the function *predict()* was used to obtain the maps.

Fitting Controls

Due to the number of parameters that need to be estimated using the two-perfusion IVIM model, there is a danger of overfitting. To avoid this and to compare IVIM and the two-perfusion IVIM models, the Akaike information criterion (AIC)[17,20] was applied corrected for small size samples. AIC is defined as:

$$\text{AIC} = N_b \ln(\text{MSE}) + \frac{2k(k+1)}{N_b - k - 1} \tag{6}$$

where N_b is the number of b-values, MSE is the mean squared error, and k is the number of the model's parameters. As shown by Riexinger et al.,[21] the comparative goodness of a model can be evaluated by considering the difference between the two competitor models' AICs (eg, $\text{AIC}_{\text{2perf}} - \text{AIC}_{\text{IVIM}}$). A negative value indicates that the first model (in the example,

15222586, 2024, 3, Downloaded from https://onlinelibrary.wiley.com/doi/10.1002/jmri.28858 by Ospedale Santa Lucia, Wiley Online Library on [04/02/2025]. See the Terms and Conditions (https://onlinelibrary.wiley.com/terms-and-conditions) on Wiley Online Library for rules of use; OA articles are governed by the applicable Creative Commons License

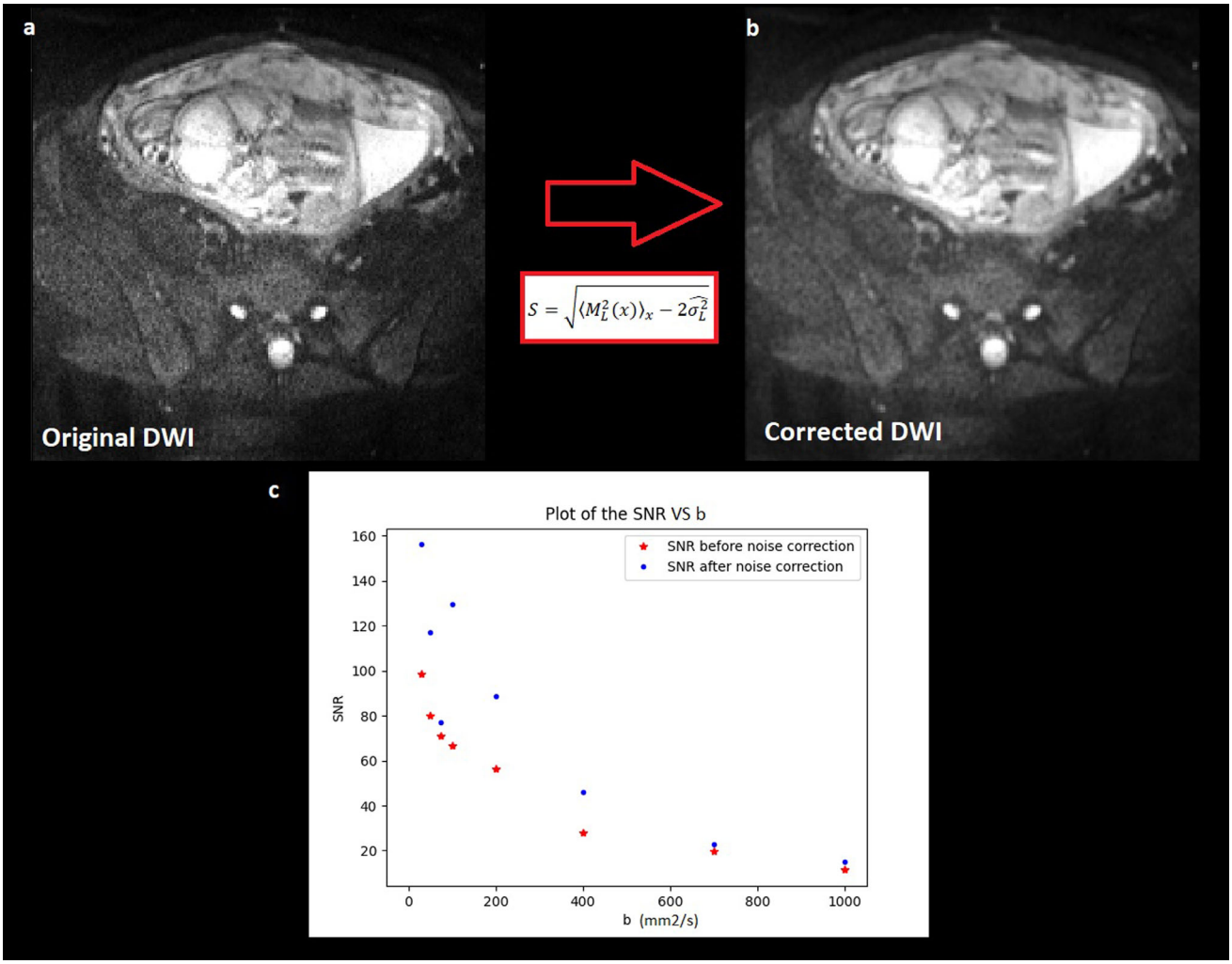

FIGURE 2: Denoising of DWI. The original DWI of a normal placenta at $b = 50$ sec/mm^2 is shown, (a); the same slice following noise correction (b). A plot of SNR vs. (b) is shown in (c).

two-perfusion) is more suitable for describing that data. The following AIC differences were calculated: $\mathrm{AIC}_{2\mathrm{perf}} - \mathrm{AIC}_{\mathrm{IVIM}} = -5.53$ and $\mathrm{IC}_{2\mathrm{perf}} - \mathrm{AIC}_{\mathrm{mono}} = -23.85$, the negative values indicating that the two-perfusion model is more suitable than the IVIM and mono-exponential models.

The Akaike weights[22] were calculated for each model as:

$$w_i(\mathrm{AIC}) = \frac{e^{-\frac{1}{2}\Delta_i(\mathrm{AIC})}}{\sum_{k=1}^{K} e^{-\frac{1}{2}\Delta_k(\mathrm{AIC})}} \qquad (7)$$

with $\Delta_i(\mathrm{AIC}) = \mathrm{AIC}_i - \min(\mathrm{AIC})$. Since the quantity $e^{-\frac{1}{2}\Delta_i(\mathrm{AIC})}$ is proportional to the likelihood of the ith model given the data $L(M_i|\mathrm{Data})$, Akaike weights can be considered as the probability that the ith model is the best model given the data and the set of models. Indeed, as shown by Fournet et al.,[17] a model's Akaike weight higher than the threshold 0.9 indicates that the model may be considered the best model of the set, and a robust inference may be possible.

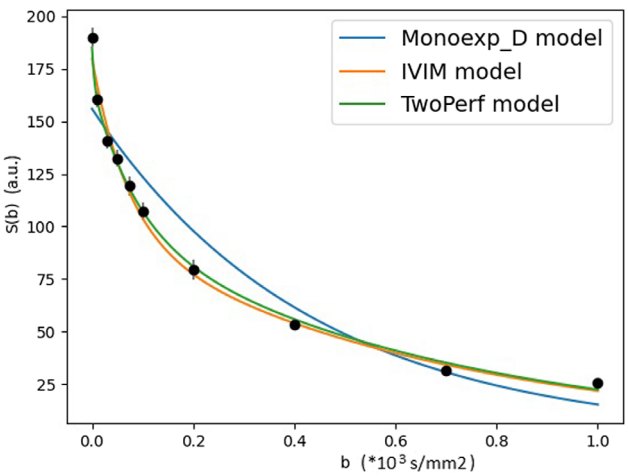

FIGURE 3: Example of a fit to DW-data obtained in the fetal ROI. The error bars were evaluated propagating the uncertainty on the noise $\widehat{\sigma_L^2}$ on the voxels inside the ROI. The Akaike weights are $w_{\mathrm{mono}}(\mathrm{AIC}) = 6.2e-06$, $w_{\mathrm{IVIM}}(\mathrm{AIC}) = 5.9e-2$, $w_{\mathrm{2perf}}(\mathrm{AIC}) = 0.94$.

15222586, 2024, 3, Downloaded from https://onlinelibrary.wiley.com/doi/10.1002/jmri.28858 by Ospedale Santa Lucia, Wiley Online Library on [04/02/2025]. See the Terms and Conditions (https://onlinelibrary.wiley.com/terms-and-conditions) on Wiley Online Library for rules of use; OA articles are governed by the applicable Creative Commons License

The Akaike weights[22] were calculated for each model (mono-exponential, IVIM, and two-perfusion) with that of the two-perfusion model being best ($w_{2perf}(AIC) = 0.94$; Fig. 3).

Statistics

Continuous variables were expressed as mean ± standard deviation. All the parameters' values obtained from each placenta group were analyzed by performing a Cohen's d test[23,24] and an ANOVA test with Dunn and Sidák's post-hoc correction (MATLAB 2021a). Since the ANOVA required the groups' homoscedasticity, a Levene test was performed to confirm the null hypothesis of equal variances across the groups. Due to the small number of placentas with different accretism, to evaluate the results obtained in accreta, increta, and percreta compared to healthy placentas, the Cohen's d effective size was used.

Regarding the correlation analysis, Spearman's coefficient was evaluated. A P-value <0.05 indicated a statistically significant difference or correlation.

Results

Examples of Two-Perfusion and IVIM Maps

Three slices from the parametric two-perfusion and IVIM maps of an example healthy placenta with GA = 22.4 weeks are shown in Fig. 4. In the first slice in Fig. 4a, the maternal side is outlined in blue, whereas the fetal side is in green; the red color outlines the umbilical cord and its insertion in the second and third slices. All the perfusion fractions f_{IVIM}, f_1 and f_2 maps (Fig. 4d,b,c, respectively) had higher values in the region of the umbilical cord insertion, and in the decidua (i.e., the maternal side), which is highly perfused by the spiral arteries. The perfusion coefficient D_2^* in Fig. 4g showed patterns, especially in the third slice where the umbilical cord insertion is far away, which were not visible in conventional IVIM D^* maps (Fig. 4h). Figure 5 shows the fetal brain of the same subject reported in Fig. 4 and shows that the two-perfusion model seems to better highlight perfusion differences in tissues than the conventional IVIM model. Indeed, in Fig. 5c the cerebral ventricles membranes clearly have higher f_2 values, whereas they are not visible in the conventional f_{IVIM} map.[25] Moreover, D_2^* (Fig. 5g) has a homogeneous value inside the ventricles.

In Fig. 6, the parametric maps of an FGR and a percreta placenta are displayed. In the DWIs shown in Fig. 6a, the placenta of the FGR subject is outlined in red, whereas the bladder of the percreta patient is outlined in yellow. In the maps of FGR, a placental lacuna is outlined in light blue, where perfusions and diffusions are higher than the surrounding tissues. The conventional IVIM D^* (Fig. 6h) does not show the placental lacuna, which is visible in all the other maps. The accretion zone of the percreta placenta is outlined in dark blue and shows high values of f_1 (Fig. 6b), whereas the bladder on the top is characterized by the lowest f_1 values (Fig. 6b). The accretion zone is also characterized by the lowest values of f_2 (Fig. 6c). Even though the accreta placenta is heterogeneous in the f_{IVIM} map (Fig. 6d), the accretion zone has fewer sharp edges compared to the f_1 and f_2 maps (shown in Fig. 6b,c, respectively). The bladder of the accreta placenta is characterized by high values of diffusion given by the urine presence (Fig. 6e), whereas it is characterized by the slowest values of D_1^* compared to the entire placenta, which is highly perfused (Fig. 6f). Finally, the D_2^* parametric map in Fig. 6g shows the lobes' structures of the accreta placenta, which are partially visible in the conventional IVIM D^* map displayed in Fig. 6h.

Two-Perfusion and IVIM Metrics

ANOVA showed that both f_2 and f_{IVIM} parameters were significantly higher in normal placentas than those in the FGR placentas (Table 2). Moreover, f_2 and f_{IVIM} were significantly higher on the fetal compared to the maternal side in normal placentas (see Fig. 7a–c and Table 2).

In Fig. 6b,c, the accretion zone has a higher value of the fastest perfusion fraction f_1 than that in the normal placenta. In particular, the entire percreta and increta placentas have the highest f_1 values (see Fig. 7d,f) with a large size effect (Cohen's $d = -2.66$, Fig. 7f). Moreover, a large effect size was found considering the discriminant power of the f_2 parameter between normal fetal and increta and percreta placenta groups (Cohen's $d = 1.12$, Fig. 7g). It was also found that f_{IVIM} is higher in the normal fetal side placenta than in the accretion zone with a small effect size ($d = 0.26$).

Perfusion fraction f_1 was significantly different between the fetal side of SGA and FGR placentas whereas there was no significant difference (P-value = 0.26) in f_{IVIM} (Fig. 7a,c).

Normal placentas had a significant negative correlation between the diffusion coefficient D and the perfusion fractions f_{IVIM} and f_2 ($\rho = -0.36$ and $\rho = -0.38$, respectively, in the fetal side and $\rho = -0.56$ and $\rho = -0.50$, respectively, in the maternal side) as shown in Fig. 8 (see also Fig. S2 and Tables S4–S6 in Supplemental Material). The accretion zone showed a significant positive correlation between the slowest perfusion fraction f_2 and the GA ($\rho = 0.90$), whereas the negative correlations between f_1 and GA ($\rho = -0.77$ and P-value = 0.05) and between f_{IVIM} and GA ($\rho = -0.63$ and P-value = 0.14) did not achieve statistical significance. The normal placenta did not show any correlation between the IVIM perfusion fraction and the gestational age ($\rho = -0.31$ and P-value = 0.051 in the fetal side and $\rho = -0.24$ and P-value = 0.12 in the maternal side) or the f_1 and the GA ($\rho = -0.24$ and P-value = 0.12 in the fetal side and $\rho = -0.13$ and P-value = 0.40 in the maternal side) or the f_2

15222586, 2024, 3, Downloaded from https://onlinelibrary.wiley.com/doi/10.1002/jmri.28858 by Ospedale Santa Lucia, Wiley Online Library on [04/02/2025]. See the Terms and Conditions (https://onlinelibrary.wiley.com/terms-and-conditions) on Wiley Online Library for rules of use; OA articles are governed by the applicable Creative Commons License

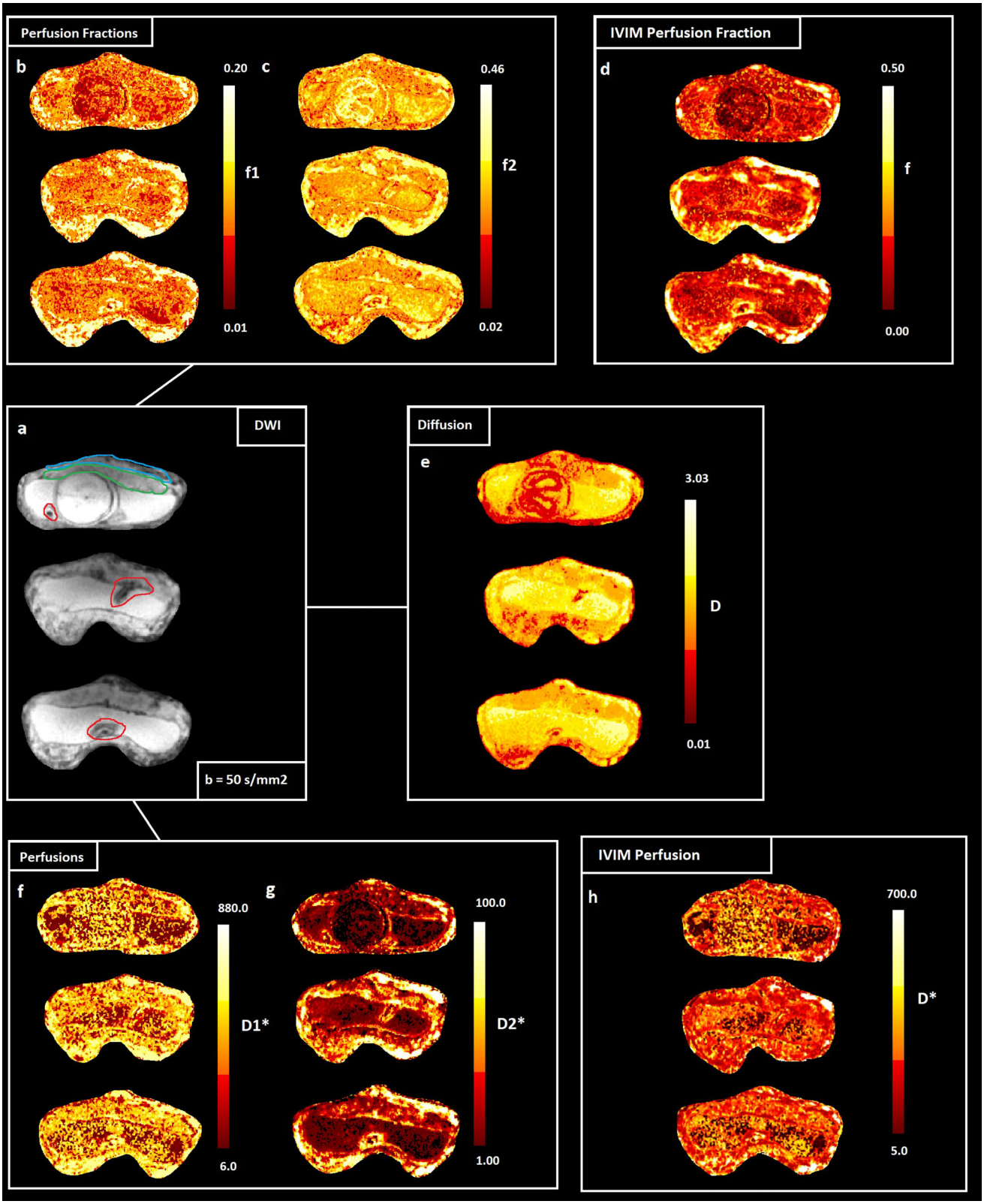

FIGURE 4: (a) The DWI section shows three different slices of the same normal placenta (GA = 22.4 weeks): the first (upper) slice shows the fetal brain, the umbilical cord (outlined in red) and a section of the placenta divided into maternal (blue) and fetal (green) sides. The second slice focuses on the umbilical cord insertion (in red), and the third slice is an overview of the entire central placenta (in red the umbilical cord). (b) f_1 parametric maps: the maternal decidua shows the highest values maybe due to the spiral arteries insertion; (c) f_2 parametric maps. (d) f_{IVIM} parametric maps; (e) The diffusion *D* maps shows high values of diffusion in the amniotic liquid as it is free water like. (f) *D*1* parametric maps; (g) *D*2* maps show interesting patterns that can be interpretated as the cotyledon structures in the placental surface. (h) *D**IVIM maps.

15222586, 2024, 3, Downloaded from https://onlinelibrary.wiley.com/doi/10.1002/jmri.28858 by Ospedale Santa Lucia, Wiley Online Library on [04/02/2025]. See the Terms and Conditions (https://onlinelibrary.wiley.com/terms-and-conditions) on Wiley Online Library for rules of use; OA articles are governed by the applicable Creative Commons License

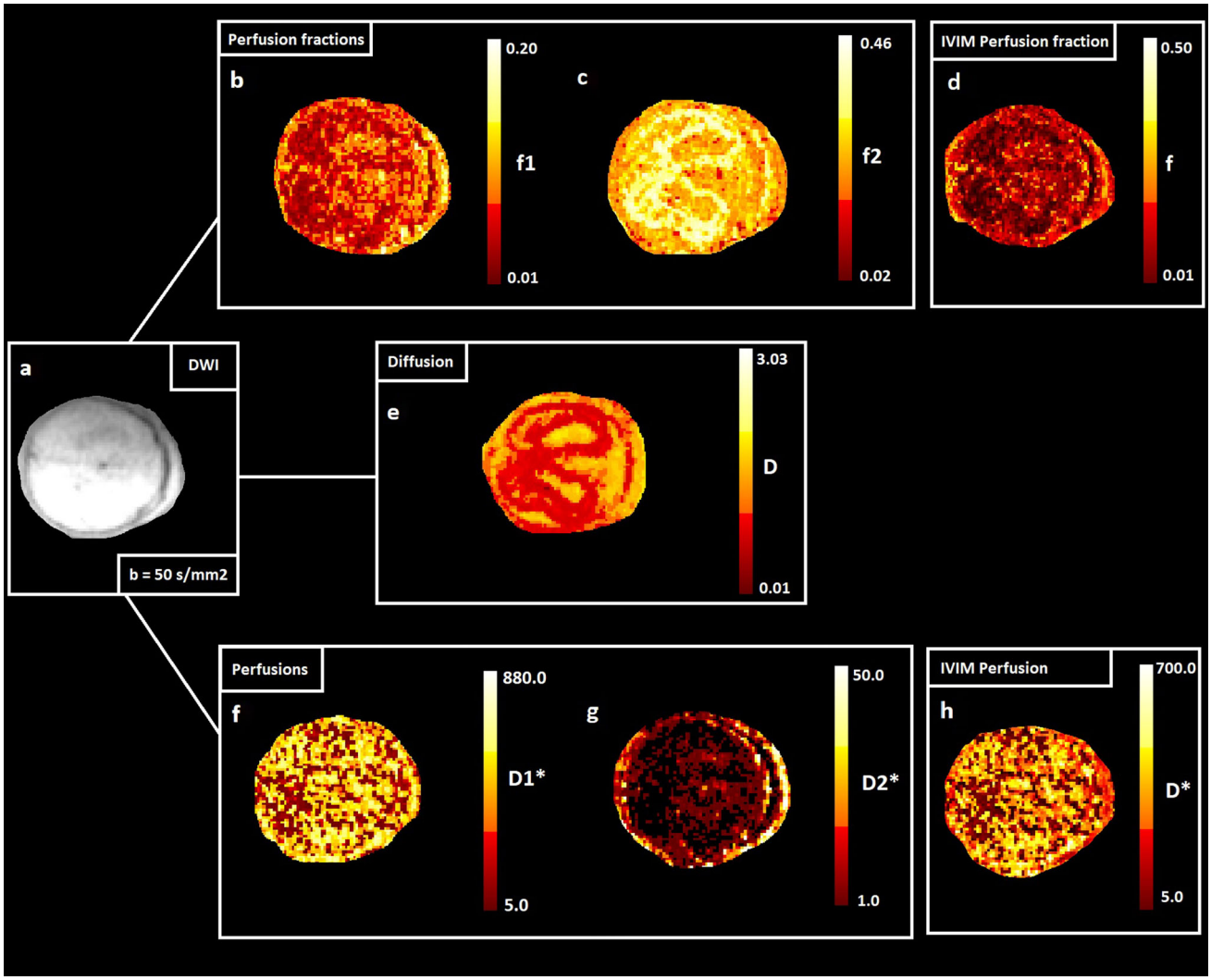

FIGURE 5: (a) Zoomed images of the fetal brain visible in the upper placenta slice of Fig. 4. (b) The f_1 map shows lower values in fetal brain compared to those in ventricular space. (c) The perfusion fraction f_2 is higher around ventricles' space, showing a probable exchange between ventricles and brain's tissues through the ventricular membrane. (d) f_{IVIM} map; (e) the diffusion coefficient *D* map. (f) *D*1* perfusion coefficient map; (g) The *D*2* perfusion coefficient map shows perfusional activity inside the ventricles; whereas, it shows lowest values in the cerebral tissue. (h) D^*_{IVIM} perfusion coefficient.

and the GA ($\rho = -0.21$ and *P*-value = 0.17 in the fetal side and $\rho = -0.22$ and *P*-value = 0.16 in the maternal side).

No significant correlations were found between *D* and GA in normal ($\rho = -0.18$ and *P*-value = 0.23 in the fetal side and $\rho = -0.05$ and *P*-value = 0.74 in the maternal side), FGR (*P*-value = 0.11 in the fetal side and *P*-value = 0.52 in the maternal side), SGA (*P*-value = 0.67 in the fetal side and *P*-value = 0.98 in the maternal side) and accreta placentas (*P*-value = 0.80 in the accretion zone).

Discussion

Since the placental tissue is a complex tissue from a vascular point of view, and most of the placental pathologies are related to vascular dysfunctions, in this work, we have used two-perfusion and IVIM metrics to better describe the complex perfusion in the placenta.

Apart from the number of subjects analyzed and the mean GA of the individual groups, our IVIM analysis of the placenta may differ from those reported in the literature due to the different types of image-denoising treatment. Subsequently, we will discuss the results obtained with the two-perfusion model highlighting the possible advantages of its use, compared to the IVIM model.

Conventional IVIM Model

The IVIM model is currently widely used in placenta MRI studies to estimate perfusion without employing exogenous contrast agents,[13,14,16,26–34] with the perfusion fraction f_{IVIM} being sensitive to changes of perfusion inside the placental tissues. In agreement with previous IVIM studies, f_{IVIM} was significantly higher on the fetal compared to the maternal side reflecting the known physiology of the organ: the placenta's fetal compartment is characterized by the villous trees, so it is

15222586, 2024, 3, Downloaded from https://onlinelibrary.wiley.com/doi/10.1002/jmri.28858 by Ospedale Santa Lucia, Wiley Online Library on [04/02/2025]. See the Terms and Conditions (https://onlinelibrary.wiley.com/terms-and-conditions) on Wiley Online Library for rules of use; OA articles are governed by the applicable Creative Commons License

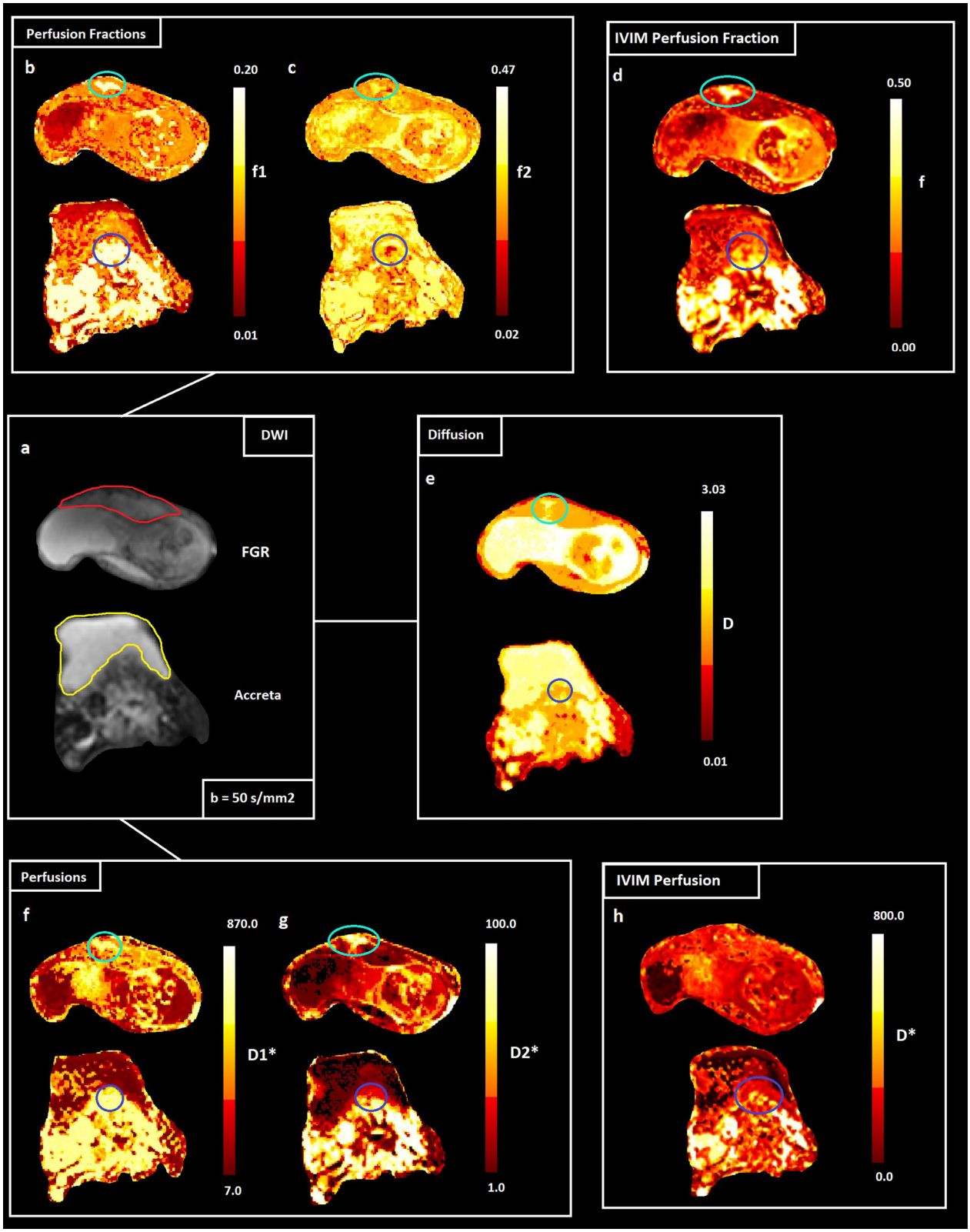

FIGURE 6: (**a**) DWI of an FGR placenta (GA = 19.7 weeks, outlined in red) and a percreta placenta with bladder infiltration (GA = 28.6 weeks, the bladder is outlined in yellow). (**b**) f_1 parametric maps: the FGR placenta shows a placental lacuna (outlined in light blue) where perfusion fraction is higher due to a placental lacuna; the accretion zone on the placenta accreta is outlined in dark blue and shows high values of f_1. (**c**) f_2 parametric maps: the FGR placenta has the highest values on the fetal side; the accretion zone (dark blue) is characterized by the slowest values of f_2. (**d**) f_{IVIM} parameter maps. (**e**) Diffusion *D* parameter maps: the placental lacuna of the FGR subject is clearly visible and this pattern could be due to the trophoblastic invasion that increases the diffusivity inside the maternal side of FGR subjects causing placental lacunae. (**f**) Perfusion coefficient *D*1* maps. (**g**) *D*2* parametric maps show the lobes' structures of the accreta subject. (**h**) IVIM *D** maps.

15222586, 2024, 3, Downloaded from https://onlinelibrary.wiley.com/doi/10.1002/jmri.28858 by Ospedale Santa Lucia, Wiley Online Library on [04/02/2025]. See the Terms and Conditions (https://onlinelibrary.wiley.com/terms-and-conditions) on Wiley Online Library for rules of use; OA articles are governed by the applicable Creative Commons License

TABLE 2. ANOVA with Dunn-Sidak Post Hoc Correction and Cohen's *d* Values

ROIs		Fetal side			Maternal side		
		f_{IVIM}	f_2	f_1	f_{IVIM}	f_2	f_1
Normal–FGR	*P*-value ANOVA D-S	**0.0042**	**0.0134**	0.8266	**0.0002**	**0.0006**	0.8076
	Cohen's *d*	1.2552	1.0757	0.2781	1.7157	1.4805	0.3044
Normal–SGA	*P*-value ANOVA D-S	0.7671	0.1642	0.0513	0.7150	0.3341	0.7597
	Cohen's *d*	0.3942	0.8642	−1.0605	0.3983	0.6789	−0.3897
FGR–SGA	*P*-value ANOVA D-S	0.2996	0.9558	**0.0386**	0.0921	0.3618	0.4885
	Cohen's *d*	−0.7314	−0.2326	−1.5209	−1.0506	−0.7530	−0.6102
Normal–Accreta		–	–	–	–	–	–
	Cohen's *d*	0.3651	1.2153	−1.3366	−0.3411	0.8733	−1.4574

Note: Statistical significant *p*-values are in bold.
FGR: fetal growth restriction; SGA: small for gestational age.

more perfused than the maternal side where the blood diffuses in the intravillous space.[26,27,35] Some studies have shown a positive or quadratic correlation between f_{IVIM} and GA in the normal placenta,[14,26,34,36] whereas other studies have found a negative correlation between f_{IVIM} and GA.[28,30] In this study, no significant correlation was found between the perfusion fraction and GA in the normal placenta, as in the study of Moore et al.[37] Indeed, Moore et al.[37] suggests that the blood volume, but also the volume of the placenta, increases with GA, so that the perfusion fraction does not change. A possible explanation for the negative correlation between f_{IVIM} and the diffusion coefficient D requires information provided by the parameter f_2 of the two-perfusion model and it will be discussed later, in the two-perfusion subsection.

In agreement with Hutter et al.,[29] no significant correlations were found between the diffusion coefficient and the GA in normal placentas.

It has previously been suggested that f_{IVIM} may be a potential marker for placental pathology such as the FGR. In previous studies, the perfusion fraction was found to be higher in normal subjects than in pathological placentas reflecting the decrease of the blood flux due to the trophoblastic infiltration.[27,30–32,34,35]

In this current study, the fetal side of normal placentas had slightly (but not significantly) higher values of perfusion fraction compared to those of the accretion zone in pathological placentas, in accordance with Bao et al.[16] who found lower values of the perfusion fraction in the placenta accreta compared to the values in a healthy pregnancy. Considering that in placenta accreta, the trophoblastic invasion extends beyond the normal limit and the placental villi are not contained in the decidual uterine cells, as is normally the case, but extend into the myometrium, the perfusion fraction was expected to be a discriminatory parameter between normal and accreta placenta.

Two-Perfusion IVIM Model

Two-perfusion maps show the potential of the two-perfusion model to highlight particular placental areas, which may be useful for diagnostic purposes or to add information not obtainable from IVIM maps.

In this study, the perfusion fraction f_2, which is related to the slowest perfusion compartment, was significantly higher on the fetal side of normal placentas than on the maternal side. This result may be interpreted by considering the trophoblastic cells: trophoblasts are responsible for nutrients exchange inside villous trees; thus, they are concentrated on the organ's fetal side. This interpretation is corroborated by the FGR placenta results. In fact, the f_2 parameter is lower in pathological subjects compared to the control group showing a lack of exchanges due to the trophoblastic infiltration on the uterine spiral arteries.[38] Moreover, a negative correlation was found between the f_2 parameter and the diffusion coefficient D on the fetal side: the trophoblastic infiltration causes an increase in the blood pressure inside the spiral arteries. This pressure increases the diffusion inside the intravillous space promoting the dispersion of nutrients and decreasing the capability of exchanges between mother and fetus. In contrast to Antonelli et al.,[33] no significant differences were found in the IVIM perfusion fraction f_{IVIM} between healthy and SGA subjects. However, the f_1 parameter was significantly different between the fetal side of FGR and SGA subjects. This result may suggest an offsetting effect, whereby the SGA placenta tries to overcome the

15222586, 2024, 3, Downloaded from https://onlinelibrary.wiley.com/doi/10.1002/jmri.28858 by Ospedale Santa Lucia, Wiley Online Library on [04/02/2025]. See the Terms and Conditions (https://onlinelibrary.wiley.com/terms-and-conditions) on Wiley Online Library for rules of use; OA articles are governed by the applicable Creative Commons License

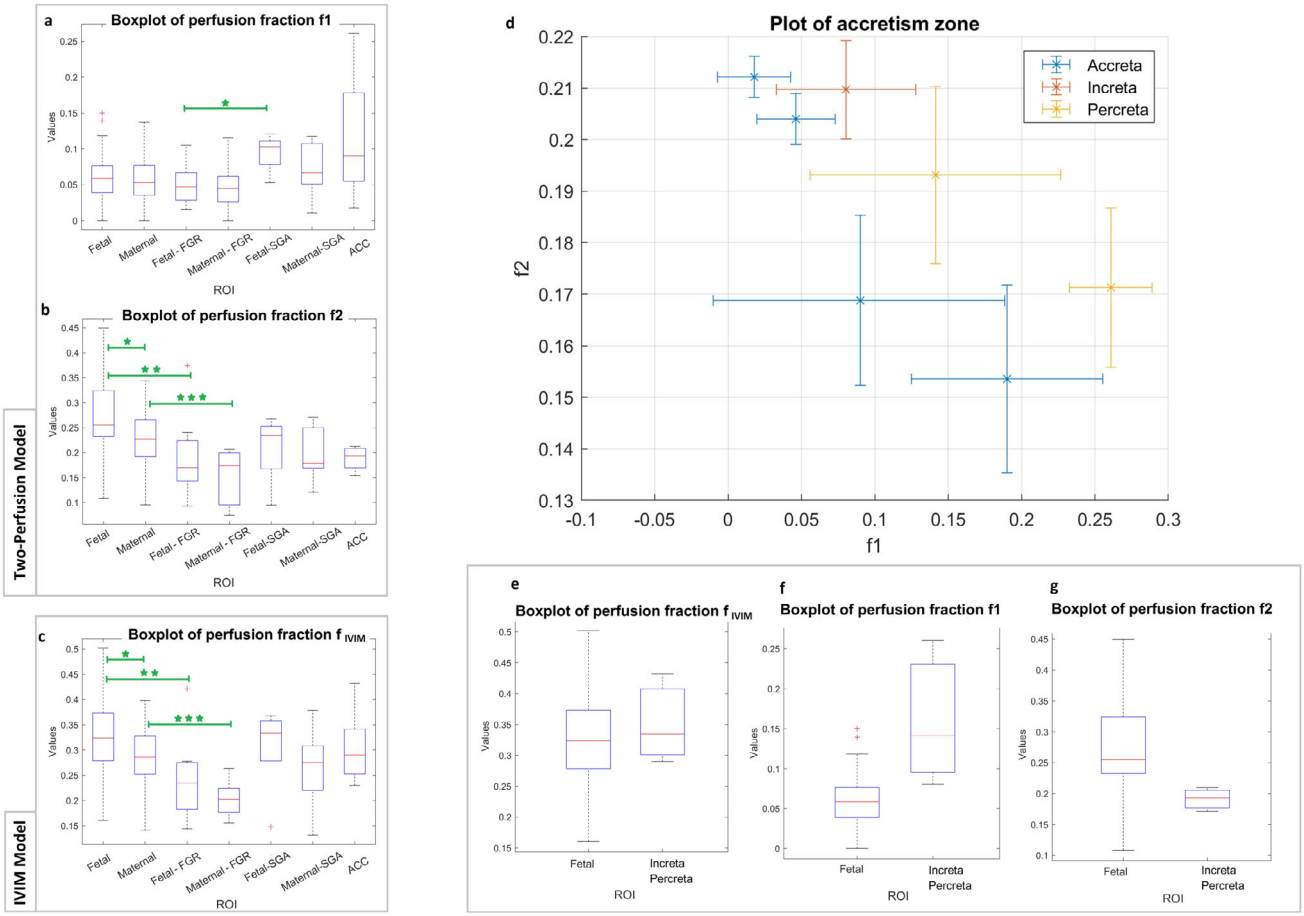

FIGURE 7: Boxplots of the perfusion fractions for the fetal and maternal placenta ROIs: (a) f_1 parameter; (b) f_2 parameter; and (c) f_{IVIM}. The group with placenta accretism was highly heterogeneous as shown in the plot of f_2 vs. f_1 (d). The percreta and increta placenta group had the highest f_1 values (d) and a large size effect (Cohen's $d = -2.66$) (f). A large effect size was also found for the f_2 parameter between the normal fetal and increta and percreta placenta groups (Cohen's $d = 1.12$) (g). (e) f_{IVIM} has a small effect size between normal and increta and percreta groups (Cohen's $d = 0.32$).

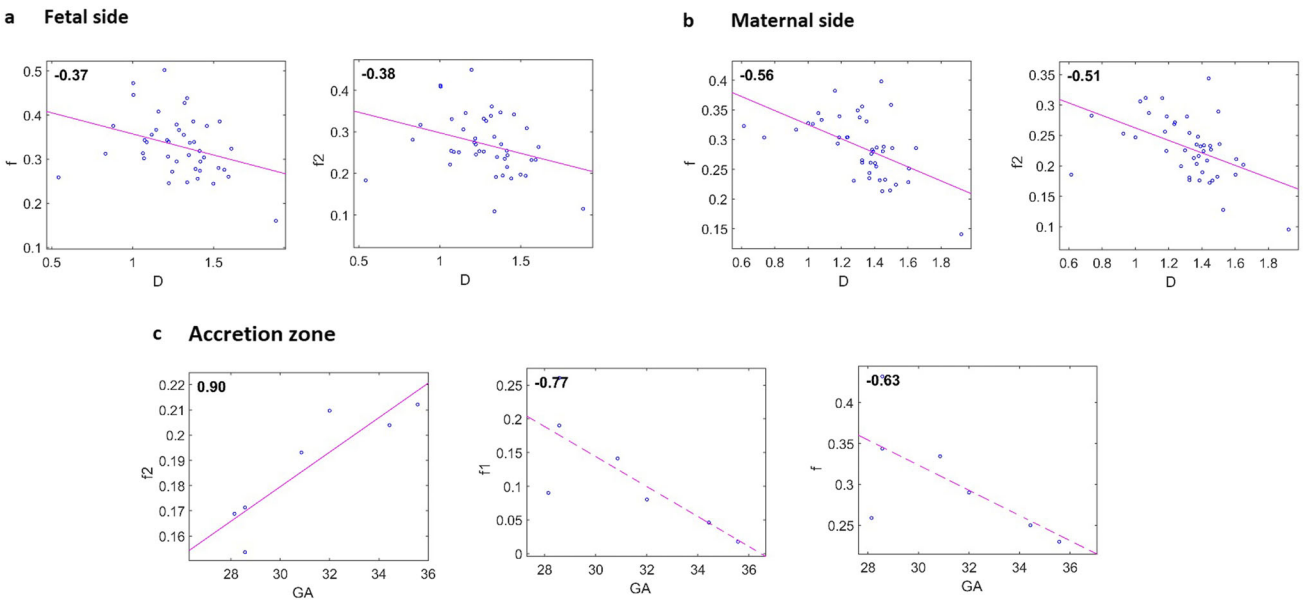

FIGURE 8: Correlation plots of healthy placentas (a,b) and of placentas with accretism (c). (a) D-f: $P < 0.05$, D-f_2: $P < 0.05$. (b) D-f: $P < 0.05$, D-f_2: $P < 0.05$. (c) GA-f_2: $P < 0.05$, GA-f_1: P-value $= 0.0532$, GA-f: P-value $= 0.1429$. The ρ value of the linear correlation is shown at the top left. The dashed line indicates a trend, while the solid line indicates a significant linear correlation.

15222586, 2024, 3, Downloaded from https://onlinelibrary.wiley.com/doi/10.1002/jmri.28858 by Ospedale Santa Lucia, Wiley Online Library on [04/02/2025]. See the Terms and Conditions (https://onlinelibrary.wiley.com/terms-and-conditions) on Wiley Online Library for rules of use; OA articles are governed by the applicable Creative Commons License

difficulty of exchange of nutrients by increasing the fetal fastest perfusion activity of the villous trees.

According to the Cohen's d, the f_1 perfusion fraction discriminates the normal pregnancies and the accreta placenta: the accretion zone is characterized by a higher value of fast perfusion fraction than the healthy subject, especially for percreta placentas where the accretism could involve surrounding organs and could cause hemorrhages during the delivery. The high values of the fastest perfusion fraction f_1 may be due to the different vascular architecture on the accretion zone.[39] Conversely, the f_2 perfusion fraction is lower in the case of accretism, showing possible impediments of slow perfusions. Although f_1 and f_{IVIM} correlated negatively with the GA, a positive correlation was found between the f_2 parameter and the GA. A possible explanation for these trends is given by the aging of the placenta. As the placenta ages, it may have less need to increase its vascularity in the anchoring area, which may bring to a decrease in the fastest perfusion activity and an increase in exchange between the infiltrating villi and the maternal blood.

The possible existence of multiple microvascular environments has been also found by Slator et al.[40]: they investigated placental tissues by simultaneously probing the diffusivity and the T2* relaxation time. The T2*-ADC spectra from the inverse Laplace transform of the signal from healthy subjects showed three separate peaks reflecting the three diffusion compartments hypothesized in the two-perfusion model. Moreover, Slator et al.[40] found the absence or reduction of one or two peaks in pathological subjects and lower values of T2* suggesting a deficiency in these compartments. This trend is in accordance with our results since we found that the slowest perfusion fraction f_2 was lower on FGR than in healthy placentas.

A later study by Slator et al.[11] suggested that anisotropic models would better describe placenta physiology. However, these need more gradient directions, which would result in an important increase in the total acquisition time of the experiment. In this work, the quantification of several perfusion and diffusion components in different placenta sites, tries to study the placenta's complex vascularization to be potentially useful for the medical diagnosis of placental impairment.

Limitations

In general, the limitations of this work are related to the limitation of IVIM technique. The most important disadvantage of the IVIM technique is the lack of standardization of the acquisition parameters and the various algorithms used for the quantitative analysis of the images. Furthermore, the sensitivity of the IVIM MRI depends on the number and the distribution of the b-values used. Therefore, due to the lack of standardization of the IVIM technique, significant variance in the calculated parameters was observed between studies, and, to date, no values for normal organs have been well established. In particular, in this work, the number of pathological subjects was low and no measure of inter-observer reproducibility was presented. Nevertheless, results reported here suggest that the two-perfusion model may be useful for studying tissues characterized by two perfusion compartments, one slower, because it is modulated by the passage of fluids through a membrane, and a faster one, in general, associated with perfusion of blood in microcapillaries.

Conclusions

The two-perfusion IVIM model, where f_1 is the fastest perfusion fraction related to perfusion in microcapillaries and villi and f_2 is the slowest perfusion fraction related to the trophoblastic cells' perfusion, may provide complementary information to IVIM parameters that may be useful in identifying placenta impairment.

References

1. Benirschke K, Burton GJ, Baergen RN. *Pathology of the human placenta*. 6th ed. Berlin: Springer; 2012.
2. Jauniaux E, Collins S, Burton GJ. Placenta accreta spectrum: Pathophysiology and evidence-based anatomy for prenatal ultrasound imaging. Am J Obstet Gynecol 2018;218(1):75-87.
3. Eriksson JG, Kajantie E, Osmond C, Thornburg K, Barker DJ. Boys live dangerously in the womb. Am J Hum Biol 2010;22(39):330-335.
4. Barker D, Osmond C, Grant S, et al. Maternal cotyledons at birth predict blood pressure in childhood. Placenta 2013;34(8):672-675.
5. Figueras F, Gardosi J. Intrauterine growth restriction: New concepts in antenatal surveillance, diagnosis, and management. Am J Obstet Gynecol 2011;204(4):288-300.
6. Gordijn SJ, Beune IM, Thilaganathan B, et al. Consensus definition of fetal growth restriction: A Delphi procedure. Ultrasound Obstet Gynecol 2016;48(3):333-339.
7. Figueras F, Eixarch E, Meler E, et al. Small-for-gestational-age fetuses with normal umbilical artery doppler have suboptimal perinatal and neurodevelopmental outcome. Eur J Obstet Gynecol Reprod Biol 2008;136(1):34-38.
8. Rizzo G, Mappa I, Bitsadze V, et al. Role of doppler ultrasound at time of diagnosis of late-onset fetal growth restriction in predicting adverse perinatal outcome: Prospective cohort study. Ultrasound Obstet Gynecol 2020;55(6):793-798.
9. Siauve N, Chalouhi GE, Deloison B, et al. Functional imaging of the human placenta with magnetic resonance. Am J Obstet Gynecol 2015; 213(4):S103-S114.
10. Amin R, Darrah T, Wang H, Amin S. Editor's highlight: in utero exposure to gadolinium and adverse neonatal outcomes in premature infants. Toxicol Sci 2017;156(2):520-526.
11. Slator PJ, Hutter J, McCabe L, et al. Placenta microstructure and microcirculation imaging with diffusion MRI. Magn Reson Med 2018;80(2): 756-766.
12. Le Bihan D, Breton E, Lallemand D, Aubin ML, Vignaud J, Laval-Jeantet M. Separation of diffusion and perfusion in intravoxel incoherent motion MR imaging. Radiology 1988;168(2):497-505.
13. Maiuro A, Antonelli A, Manganaro L, Capuani S. Molecular diffusion and perfusion of biological water quantified by MRI for the diagnosis of pathological human placentas. Il Nuovo Cimento 2020;43(4–5):1-5.
14. Siauve N, Hayot PH, Deloison B, et al. Assessment of human placental perfusion by intravoxel incoherent motion MR imaging. J Matern Fetal Neonatal Med 2019;32(2):293-300.

15222586, 2024, 3, Downloaded from https://onlinelibrary.wiley.com/doi/10.1002/jmri.28858 by Ospedale Santa Lucia, Wiley Online Library on [04/02/2025]. See the Terms and Conditions (https://onlinelibrary.wiley.com/terms-and-conditions) on Wiley Online Library for rules of use; OA articles are governed by the applicable Creative Commons License

15. Andescavage N, You W, Jacobs M, et al. Exploring in vivo placental microstructure in healthy and growth-restricted pregnancies through diffusion-weighted magnetic resonance imaging. Placenta 2020;93: 113-118.

16. Bao Y, Pang Y, Sun Z, Li Q, Tang D, Xia L. Functional diagnosis of placenta accreta by intravoxel incoherent motion model diffusion-weighted imaging. Eur Radiol 2021;31:740-748.

17. Fournet G, Li J-R, Cerjanic AM, Sutton BP, Ciobanu L, Le Bihan D. A two-pool model to describe the IVIM cerebral perfusion. J Cereb Blood Flow Metab 2017;37(8):2987-3000.

18. Solomon E, Avni R, Hadas R, et al. Major mouse placental compartments revealed by diffusion-weighted MRI, contrast-enhanced MRI, and fluorescence imaging. Proc Natl Acad Sci USA 2014;111(28): 10353-10358.

19. Aja-Fernández S, Tristán-Vega A, Alberola-López C. Noise estimation in single- and multiple-coil magnetic resonance data based on statistical models. Magn Reson Imaging 2009;27(10):1397-1409.

20. Akaike H. A new look at the statistical model identification. IEEE Trans Automat Contr 1974;19(6):716-723.

21. Riexinger A, Martin J, Wetscherek A, et al. An optimized b-value distribution for triexponential intravoxel incoherent motion (IVIM) in the liver. Magn Reson Med 2021;85(4):2095-2108.

22. Wagenmakers EJ, Farrell S. AIC model selection using Akaike weights. Psychon Bull Rev 2004;11:192-196.

23. Cohen J. *Statistical power analysis for the behavioral sciences*. revised ed. New York: Academic Press; 1977.

24. Sawilowsky SS. New effect size rules of thumb. J Mod Appl Stat Methods 2009;8(2):597-599.

25. Di Trani MG, Manganaro L, Antonelli A, et al. Apparent diffusion coefficient assessment of brain development in normal fetuses and ventriculomegaly. Front Phys 2019;7:160.

26. Capuani S, Guerreri M, Antonelli A, et al. Diffusion and perfusion quantified by magnetic resonance imaging are markers of human placenta development in normal pregnancy. Placenta 2017;58:33-39.

27. Moore R, Strachan B, Tyler D, et al. In utero perfusing fraction maps in normal and growth restricted pregnancy measured using IVIM echo-planar MRI. Placenta 2000;21(7):726-732.

28. Moore R, Issa B, Tokarczuk P, et al. In vivo intravoxel incoherent motion measurements in the human placenta using echo-planar imaging at 0.5 T. Magn Reson Med 2000;43(2):295-302.

29. Hutter J, Slator PJ, Jackson L, et al. Multi-modal functional MRI to explore placental function over gestation. Magn Reson Med 2019; 81(2):1191-1204.

30. Sohlberg S, Mulic-Lutvica A, Olovsson M, et al. Magnetic resonance imaging-estimated placental perfusion in fetal growth assessment. Ultrasound Obstet Gynecol 2015;46(6):700-705.

31. Sohlberg S, Mulic-Lutvica A, Lindgren P, Ortiz-Nieto F, Wikström AK, Wikström J. Placental perfusion in normal pregnancy and early and late preeclampsia: A magnetic resonance imaging study. Placenta 2014; 35(3):202-206.

32. Avni R, Neeman M, Garbow JR. Functional MRI of the placenta–from rodents to humans. Placenta 2015;36(6):615-622.

33. Antonelli A, Capuani S, Ercolani G, et al. Human placental microperfusion and microstructural assessment by intra-voxel incoherent motion MRI for discriminating intrauterine growth restriction: A pilot study. J Matern Fetal Neonatal Med 2022;35(25):9667-9674.

34. Derwig I, Lythgoe D, Barker G, et al. Association of placental perfusion, as assessed by magnetic resonance imaging and uterine artery doppler ultrasound, and its relationship to pregnancy outcome. Placenta 2013; 34(10):885-891.

35. You W, Andescavage N, Zun Z, Limperopoulos C. *Medical imaging 2017: Biomedical applications in molecular, structural, and functional imaging*. Vol 10137. Bellingham, WA, USA: International Society for Optics and Photonics; 2017.

36. Jakab A, Tuura RL, Kottke R, et al. Microvascular perfusion of the placenta, developing fetal liver, and lungs assessed with intravoxel incoherent motion imaging. J Magn Reson Imaging 2018;48(1):214-225.

37. Moore RJ, Ong SS, Tyler DJ, et al. Spiral artery blood volume in normal pregnancies and those compromised by pre-eclampsia. NMR Biomed 2008;21(4):376-380.

38. Moffett-King A. Natural killer cells and pregnancy. Nat Rev Immunol 2002;2(9):656-663.

39. Chantraine F, Blacher S, Berndt S, et al. Abnormal vascular architecture at the placental-maternal interface in placenta increta. Am J Obstet Gynecol 2012;207(3):188.e1-188.e9.

40. Slator PJ, Hutter J, Palombo M, et al. Combined diffusion-relaxometry MRI to identify dysfunction in the human placenta. Magn Reson Med 2019;82(1):95-106.

15222586, 2024, 3, Downloaded from https://onlinelibrary.wiley.com/doi/10.1002/jmri.28858 by Ospedale Santa Lucia, Wiley Online Library on [04/02/2025]. See the Terms and Conditions (https://onlinelibrary.wiley.com/terms-and-conditions) on Wiley Online Library for rules of use; OA articles are governed by the applicable Creative Commons License